Ecological Engineering 169 (2021) 106306

Contents lists available at ScienceDirect

Ecological Engineering

journal homepage: www.elsevier.com/locate/ecoleng

Detecting hydrodynamic changes after living shoreline restoration and through an extreme event using a Before-After-Control-Impact experiment

David W. Spiering [a,*], Kelly M. Kibler [a,b], Vasileios Kitsikoudis [a,c], Melinda J. Donnelly [d], Linda J. Walters [b,d]

[a] Department of Civil, Environmental, and Construction Engineering, University of Central Florida, Orlando, FL 32816, USA
[b] National Center for Integrated Coastal Research, 4000 Central Florida Blvd., Orlando, FL 32816, USA
[c] Water Engineering and Management, Faculty of Engineering Technology, University of Twente, Enschede, The Netherlands
[d] Department of Biology, University of Central Florida, Orlando, FL 32816, USA

ARTICLE INFO

Keywords:
Living shorelines
Hydrodynamics
Spartina alterniflora
Mangroves
Turbulence
Hurricane Irma

ABSTRACT

Stabilization of eroding estuarine shorelines using living shoreline techniques, including native vegetation and nearshore structural components, has the potential to combat erosion while increasing shoreline ecotone function. However, there are few detailed field studies and little quantitative data available to assess hydrodynamic changes that occur immediately following living shoreline implementation. To address this gap, detailed hydrodynamic observations were made along eroding and stable reference shorelines over a 16-month period spanning living shoreline stabilization, which included the landfall of a major hurricane (Irma) 9 weeks after stabilization. In the months following stabilization, planted vegetation was sparse and shoreline hydrodynamics were governed by water level relative to breakwater structures. When water levels were at or below breakwater crest elevation, current velocities were initially reduced by 62% and wave heights by up to 83%; however, at higher water levels, shoreline velocities at the stabilized site vastly exceeded those observed at a nearby bare control site. Sixteen months after stabilization, flow-vegetation interactions had become a dominant control over shoreline hydrodynamics, and current attenuation was similar to that observed in nearby mature mangrove vegetation. Additionally, turbulence dissipation rates at the stabilized site ($2.2 \cdot 10^{-5}$ m^2/s^3) and vegetated reference site ($1.1 \cdot 10^{-5}$ m^2/s^3) were an order of magnitude greater during boat wake events compared to the bare shoreline site ($1.6 \cdot 10^{-6}$ m^2/s^3, $p < 0.001$). This first experimental assessment of hydrodynamic effects related to living shoreline stabilization indicates that more than one year may be required before planted vegetation meaningfully influences shoreline hydrodynamics.

1. Introduction

Wetland and estuarine habitats such as marshes, coral and shellfish reefs, and mangrove forests provide a multitude of critical ecosystem services (Mcleod et al., 2011; Barbier et al., 2011; Grabowski et al., 2012) which, if incorporated into coastal planning, provide numerous benefits (Arkema et al., 2015). Given the increasing frequency and severity of hydrologic events and projected acceleration of sea level rise (Nicholls et al., 1999; Nicholls and Cazenave, 2010; Nicholls and Cazenave, 2010; Tebaldi et al., 2012; Stocker et al., 2013) and that over 10% of the world's population lives within 10 m of mean sea level (McGranahan et al., 2007), protection of vulnerable coastal regions is vital. In addition to climatic variability, aquatic recreational activities may exacerbate shoreline erosion, as wakes generated by boating activity may introduce high-magnitude forces to shorelines (McConchie and Toleman, 2003; Herbert et al., 2018), leading to ecosystem degradation (Wall et al., 2005; Campbell, 2015). Reinforcement of shorelines is therefore often necessary to limit erosion and preserve ecosystems.

Traditional strategies for shoreline protection often involve hardened structures (e.g. bulkheads, seawalls, revetments) which introduce above-equilibrium slopes, change local hydrodynamics (Miles et al., 2001), and modify sediment transport and nearshore morphology (Plant and Griggs, 1992; Griggs, 2005). Additionally, seawalls and bulkheads effectively eliminate the intertidal ecotone, reducing shoreline biodiversity and wetland habitat (Bozek and Burdick, 2005; Gittman et al., 2016a) and lowering potential for biogeochemical transformations in

* Corresponding author.
E-mail address: dwspiering@gmail.com (D.W. Spiering).

https://doi.org/10.1016/j.ecoleng.2021.106306
Received 20 April 2020; Received in revised form 4 June 2021; Accepted 6 June 2021
Available online 21 June 2021

the shoreline ecotone (Vidon and Hill, 2004; Dosskey et al., 2010). As wetlands are recognized as a crucial component of the biological carbon pool (Chmura et al., 2003), ecosystem services related to sequestration of carbon (Chmura, 2009; Mcleod et al., 2011; Mitra and Zaman, 2015; Ridge et al., 2017) are largely eliminated along hardened shorelines.

Trends in shoreline stabilization have shifted toward nature-based approaches utilizing native vegetation and materials produced by living organisms (e.g. biogenic breakwaters) (Bilkovic et al., 2017). Living shoreline methods aim to promote natural ecotone processes while stabilizing eroding shorelines (Coen et al., 1999; Gittman et al., 2016b; Polk and Eulie, 2018; Morris et al., 2019) through reduction of hydrodynamic energy and trapping of sediment (Piazza et al., 2005; (Gedan et al. 2011; Horstman et al., 2014). Use of native wetland vegetation to stabilize eroding shorelines is supported by scientific literature regarding flow-vegetation-sediment interaction (Bouma et al., 2005; Temmerman et al., 2005; Larsen and Harvey, 2010). Emergent vegetation increases drag on flow, reducing mean velocities and wave heights (Nepf, 1999; Horstman et al., 2012, 2013), while eddies generated downstream of individual stems increase turbulence (Nepf, 2012). However, the net effect to sediment transport from the combination of reduced flow velocity and increased instantaneous shear stresses due to turbulent bursts depends on vegetation characteristics, such as density, size, configuration and rigidity of plant elements (Yager and Schmeeckle, 2013; Yang and Nepf, 2018, Yagci et al., 2017). Neumeier and Amos (2006) observed that bed turbulence was reduced within emergent vegetation (*Spartina alterniflora*) due to lower flow velocities, suggesting that this interaction might enhance sediment deposition. However, Tinoco and Coco (2018) observed that turbulence generated from the interaction of emergent stems with oscillatory flow led to sediment suspension. Norris et al. (2017) found that turbulence intensity produced by interactions with mangrove pneumatophores was greatest at the fringe and that dissipation scaled correspondingly with increased vegetation density. Similarly, Kibler et al. (2019) observed that turbulence dissipation rates were greater in dense mature mangrove in a natural shoreline fringe as compared to within a living shoreline planted with marsh grasses and young mangroves. However, more than 6 years after living shoreline stabilization, flow patterns within the Restored shoreline were more similar to the natural mangrove shoreline than to a bare shoreline with a seawall, highlighting the potential impact of successful shoreline restoration on local hydrodynamics.

While the aims of living shoreline stabilization are multi-faceted, much available data focus on ecological impacts (Scyphers et al., 2011; La Peyre et al., 2014; Davis et al., 2006). Because overall effects to hydrodynamics and sediment transport by vegetation are highly context-specific and field observation of nearshore hydrodynamics in living shorelines are rare, many process-level questions remain unanswered. For instance, understanding the precise mechanisms by which living shorelines affect hydrodynamics and sediment transport, particularly at early stages when new plantings may be sparse and most susceptible to failure, are critical to design of more robust green infrastructure. The objective of this study is to observe changes in shoreline hydrodynamics during early stages of living shoreline implementation. A Before-After-Control-Impact (BACI) experimental design is applied over 16 months, which includes the implementation of a living shoreline and landfall of a major hurricane. Hydrodynamic changes at the living shoreline site are compared to those occurring simultaneously in controlled reference-condition and degraded shorelines. We address the hypothesis that hydrodynamic and related benthic sediment changes within the living shoreline exceed natural variability observed within nearby bare shoreline that is not restored. This is the first such experimental assessment of hydrodynamic effects related to living shoreline stabilization.

2. Methods

2.1. Study location and experimental design

Three shoreline study sites were selected from the east bank of Mosquito Lagoon, a shallow (mean water depth < 3 m), microtidal estuary located on the Atlantic coast of Florida, USA (Fig. 1a), where rates of relative sea level rise are around 2.4 mm/yr (Maul, 2015). Berms created in conjunction with historical mosquito impoundments have artificially steepened shoreline slopes in Mosquito Lagoon (Brockmeyer et al., 1996) and loss of wetland vegetation and erosion is widespread. The sites were selected due to their location along a continuous span of shoreline, a portion of which was restored during the experiment as part of a community-based restoration project. The study region has a subtropical climate with annual mean precipitation of 125 cm, most of which occurs during a rainy season from May to October. Estuarine salinities vary with rainfall and tidal influences but may reach up to 40 ppt (Down and Withrow, 1978; Walters et al., 2001). Common shoreline species in Mosquito Lagoon include oyster (*Crassostrea virginica*), emergent marsh grasses *Spartina alterniflora* and *Rhizophora mangle* (red mangrove) at the seaward edge. Moving inland to the supratidal zone, vegetation transitions to *Avicennia germinans* (black mangrove) and *Laguncularia racemosa* (white mangrove).

The study sites (Fig. 1b-g, each approximately 75 m) included 1) an actively eroding shoreline with unvegetated intertidal zone (Control site), 2) a stable shoreline, with a dense stand of red, black, and white mangroves extending into the subtidal zone (Reference site), and 3) an unvegetated, actively degrading shoreline that was restored during this experiment using living shoreline techniques (Restored site). The Restored shoreline was stabilized on July 6, 2017 with a biogenic breakwater structure and planted vegetation. The structure was constructed of polyethylene mesh bags filled with disarticulated oyster shell. Oyster shell bags (90 cm length, 35 cm width, 25 cm height) were stacked in a double layer and joined together to create structures measuring approximately 6 m long, by 0.90 m wide, by 0.50 m high. Structures were placed within the lower limits of the intertidal zone, approximately 3–5 m from the shoreline slope break. As required by permitting conditions, 2 m gaps were placed between each 6 m structure (Fig. 2), to facilitate passage for aquatic life. Ten 1-gal pots of *S. alterniflora* and eight 3-year old *A. germinans*, *L. racemosa*, and *R. mangle* were planted by community volunteers behind each 6 m span of structure. Over 2.65 km of shoreline were planned and permitted for this restoration effort, which has been undertaken in stages over several years. The implementation studied and reported herein consisted of nine 6-m spans of breakwater structure and associated vegetation.

Hydrodynamic observations were collected over flood tides (approximately 4-h periods) at each site: before restoration (June 2017), directly after restoration (July 2017), approximately 4 months after the restoration (November 2017), and 16 months after restoration (November 2018). Observation periods were selected to test for hydrodynamic effects at variable water levels, with summer samplings reflecting annual low water levels and fall samplings reflecting annual peak water levels. An attempt was made to record hydrodynamic data 12 months after restoration; however, water levels in the Restored shoreline were insufficient to sample due to deposition of sediments. Hurricane Irma made landfall in Florida as a category 3 hurricane approximately 2 months after restoration on September 10, 2017. Sustained wind speeds at Cape Canaveral were 104 km/h with gusts of 122 km/h and storm surges were recorded at 3 to 5 ft of inundation above ground level (Cangialosi et al., 2018). Flooding within the study area was sustained and post-event sampling occurred within weeks of the extreme event, as soon as study sites could be safely accessed.

2.2. Data collection

High-frequency velocity and wave measurements were conducted on

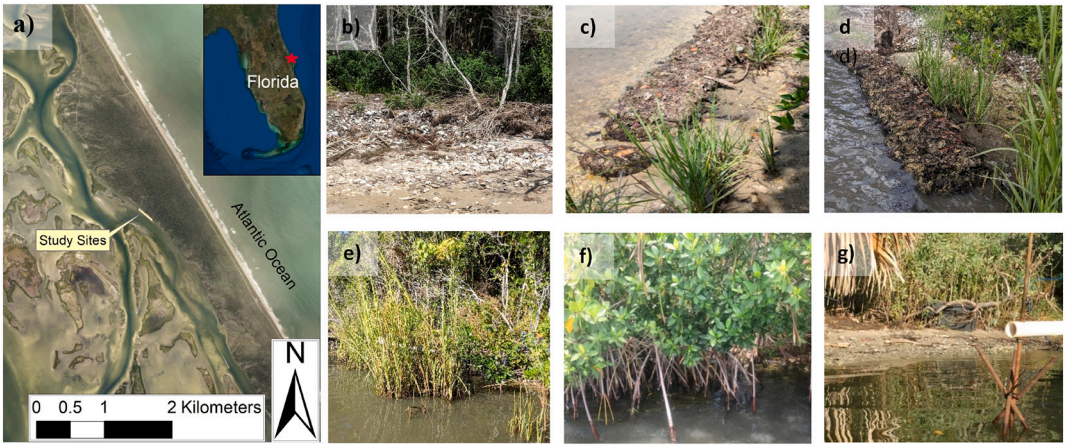

Fig. 1. Study site within (a) Florida's Mosquito Lagoon and sampling locations: Restored shoreline (b) before restoration, (c) 1 month after restoration, (d) 4 months after restoration, (e) 16 months after restoration, (f) Reference shoreline (g) Control shoreline.

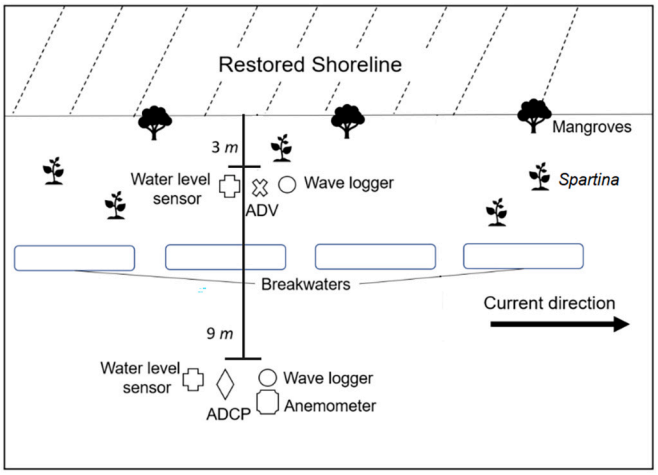

Fig. 2. Example sitemap with instrumentation placement and restoration layout relative to the upper intertidal shoreline slope break. Instrumentation placements were replicated in the Control and Reference sites.

shorelines of each site and simultaneously within the nearby channel (Fig. 2). Flow velocities on shorelines were observed 4–6 cm above the bed using a Nortek Vectrino Profiler, configured such that *u*, *v*, *w* corresponded to alongshore, cross-shore, and vertical directions, respectively. The instrument was levelled and configured to record a 3-cm velocity profile with a 1 mm cell size at a continuous rate of 100 Hz. Water surface deformation was observed at 32 Hz using acoustic wave sensors (Ocean System Sensors, Sonic Wave XB). Water levels were observed at a frequency of 0.1 Hz using HOBO U20L-004 water level loggers. Shoreline hydrodynamic data were collected in similar water depths (10–17 cm), 3–5 m seaward from the shoreline slope break. Vegetation conditions in the intertidal zone of study sites varied from site to site, and over time in the Restored site. The intertidal zone of the Control shoreline contained no wetland vegetation and consisted of bare sediments for the duration of the experiment. Within the Reference shoreline, instruments were placed within mature red mangrove (*R. mangle*) prop roots. At the Restored site, hydrodynamics were observed within the unvegetated intertidal zone before restoration and landward of the breakwater structure within planted vegetation after restoration. Sensors were positioned such that vegetation did not directly enter the sampling volumes, but fluid within the sampling volumes reflected flow interaction effects of the surrounding vegetation. No clearing of vegetation was necessary to achieve this.

Within a 0.25 m^2 quadrat centered around the location of shoreline hydrodynamic data collection, stem density, species and diameter were recorded. Each stem in the quadrat was measured at the water surface using calipers. Vegetation cover was additionally monitored at the site scale before restoration, one month after restoration, and every three months after restoration up to and including 15 months post-restoration. Two 7-m line transects per site were run perpendicular to the shoreline from the subtidal zone landward through the upper intertidal zone. Percent vegetation cover was assessed along every meter with a 0.25 m^2 quadrat using the point-intercept method.

Channel velocity data were collected offshore in 0.6–0.9 m of water using a Nortek Aquadopp acoustic Doppler current profiler (ADCP). The instrument was levelled and positioned down-looking just below the water surface. Data were sampled at 2 Hz with a cell size of 15–20 mm and the coordinate system was set to match that of the shoreline velocity sensor. A wave sensor and water level logger were co-located with the channel ADCP, positioned similarly to the shoreline sensors. Wind data were measured using a Davis Vantage Pro 2 anemometer and HoboWare data logger collecting wind data at a resolution of 0.1 Hz.

Hydrodynamic data were recorded to assess shorelines during ambient environmental conditions and during controlled boat passes. During ambient data collection, uncontrolled boat passes were noted and data reflecting wake conditions were omitted. Boating activity can generate high-magnitude wake events which may differ considerably from ambient wind-generated waves and may occur with sufficient frequency to potentially be a dominant control to shoreline sediment transport processes (Herbert et al., 2018; Garvis et al., 2015). Assessment of performance by living shorelines to mitigate boat wakes is of value. To understand boat wake effect to shoreline hydrodynamics, a series of ten controlled boat passes were conducted approximately 25 m offshore of each site 16 months after restoration. A 6-m long Carolina Skiff (flat hull) outfitted with a 90 HP outboard motor was used to complete passes on plane at speeds of ~35 knots.

Each shoreline was surveyed along 40 m transects from the shoreline slope break into the channel utilizing a CHC X91+ Real Time Kinematic (RTK) GPS survey device. Bulk sediment samples were collected in all shorelines and channels at both low and high water levels to assess spatial and temporal variation in bed sediments. At each site, five replicate bulk samples (10–15 cm) were extracted using a manual gravity core system on the shoreline and within the channel. Overlying water was collected with the sediments which were subsequently processed for grain size distribution and organic matter content (further detailed in Supplemental Material).

2.3. Hydrodynamic data analysis

Raw velocity data from both channel and shoreline velocity sensors were averaged over 120 s moving averages with a 30 s overlap. Signal-to-noise (SNR) ratio and correlation of shoreline measurement were high, with mean values generally around 35 dB and 95%, respectively. Outliers were filtered using the phase-space method (Goring and Nikora, 2002; Wahl, 2003). Channel velocity measurements had correlations greater than 70%. Depth-integrated channel velocities were calculated over each 120 s time-interval.

Turbulence dissipation rates (ε) were assessed for both ambient conditions and boat wake passes using the structure function method adapted for ADCP measurements by Wiles et al. (2006). Details on application of the structure function method to similar flow profiles can be found in Kitsikoudis et al. (2020) and Norris et al. (2019). For ambient measurements, dissipation rates were calculated as moving averages across 120 s intervals. For measurements from experimental boat wakes, a 5 s time window with a 2.5 s increment was applied to obtain mean dissipation values over each wake event, as applied by Lanckriet and Puleo (2013) for measurements in the swash zone. Cells at profile ends were excluded from structure function analysis to ensure sufficient accuracy (Thomas et al., 2017). Time-intervals that exhibited low data quality were discarded from the analysis and ε values were not calculated. To account for variation in dissipation rates from differences in conditions (velocities, waves) among sites and days, dissipation rates were normalized by the root-mean-square velocity, $u_{rms} = \sqrt{\overline{u^2}}$, similar to Stocking et al. (2016), yielding a ratio of dissipation to quadratic mean velocity. Additional methodology is further detailed in Supplemental Material.

Wave data were filtered to replace outliers falling more than 10 standard deviations from a mean computed across a moving window of each 50 samples (1.6 s) with median values. Filtered data were processed using a smoothing function over 50 samples (0.16 s) to remove spurious data not associated with discernible periodic waves. Smoothed data were sorted into the 120 s moving average segments, incremented by 30 s, over which wave statistics were computed. A zero upcrossing method was used to isolate individual waves within the smoothed data. Significant wave heights (H_S) and their corresponding significant wave periods (T_S) were determined from the mean of the largest 33% of identified waves in each moving average segment.

Data were evaluated to confirm assumptions of normal distribution and heterogeneity of variances. Current and wave attenuation and turbulence dissipation rates were compared using one-way analysis of variance (ANOVA) followed by Tukey post hoc pairwise comparisons to identify statistical significance ($\alpha = 0.05$) between study sites (Table 1, Table A4).

3. Results

3.1. Shoreline velocities

Mean depth-integrated channel velocities ranged from 2 to 9 cm/s in summer (low water levels) and from 8 to 16 cm/s in fall (high water levels) (Table 2, Fig. 3). Prior to restoration, mean near-bed horizontal velocities observed at the degraded Restored shoreline (0.5 ± 0.4 cm/s) were similar to those observed at the neighboring Control site (0.3 ± 0.3 cm/s), and velocity attenuation rates were slightly higher from the channel to the Control shoreline (Fig. A3a). Shoreline velocities in the vegetated Reference shoreline were the lowest among all sites, and velocity attenuation from the channel was greatest (drop from 9.1 ± 2.1 cm/s in channel to 0.2 ± 0.1 cm/s in shoreline). Immediately following restoration, mean near-bed velocities at the Restored shoreline decreased by 62% despite no change in channel velocities (Fig. A3b).

All components of the living shoreline were intact four months after restoration and two months after Hurricane Irma. During seasonal high water levels, channel velocities were greater in all sites. Mean depth-integrated channel velocities were greatest off the Reference (16.3 ± 0.5 cm/s) and Restored sites (12.8 ± 1.1 cm/s), and increased less dramatically at the Control site (8.0 ± 1.5 cm/s). Despite this, mean velocities observed in the Restored shoreline (5.7 ± 0.5 cm/s) were an order of magnitude greater than shoreline flows in either the Reference (0.7 ± 0.1 cm/s) or Control (0.4 ± 0.1 cm/s) shorelines (Fig. 3, Fig. A4). Sixteen months after restoration, at seasonal high water levels, mean near-bed velocities observed at the Restored shoreline (0.2 ± 0.1 cm/s) were the lowest observed across the sites, with channel velocities of 11.4 ± 0.8 cm/s (Table 2, Fig. 3, Fig. A4). Reference shoreline velocities were also low (0.4 ± 0.1 cm/s) with slightly greater channel velocities (13.7 ± 0.5 cm/s). Control shoreline velocities were higher (0.6 ± 0.7

Table 2
Mean ± 1 SD observed channel and shoreline velocities and mean current attenuation over sampling period.

	Site	*u* Channel (cm/s)	*u* Shoreline (cm/s)	Mean Current Attenuation (%)
Before restoration (low water season)	Restored	2.1 ± 1.2	0.5 ± 0.4	47.3
	Control	5.8 ± 0.5	0.3 ± 0.3	89.6
	Reference	9.1 ± 2.1	0.2 ± 0.1	98.0
1 month after restoration (low water season)	Restored	2.1 ± 1.5	0.2 ± 0.1	87.9
	Control	*	0.5 ± 0.4	*
	Reference	5.9 ± 1.1	0.1 ± 0.1	97.9
4 months after restoration (high water season)	Restored	12.8 ± 1.1	5.7 ± 0.5	55.11
	Control	8.0 ± 1.5	0.4 ± 0.1	93.2
	Reference	16.3 ± 0.5	0.7 ± 0.1	96.0
16 months after restoration (high water season)	Restored	11.4 ± 0.8	0.2 ± 0.1	98.2
	Control	11.9 ± 0.4	0.6 ± 0.7	95.7
	Reference	13.7 ± 0.5	0.4 ± 0.1	97.6

Table 1
Pairwise comparisons of current and wave attenuation rates from channel to shore, and normalized turbulence dissipation at the Restored, Control, and Reference sites.

		Current Attenuation		Normalized Turbulence Dissipation		Wave Attenuation	
		Mean Difference ± SE (%)	*p*-value	Mean Difference ± SE (%)	p-value	Mean Difference ± SE (%)	p-value
Jun 2017	Control-Reference	8.4 ± 0.067	0.634				
	Control-Restored	42 ± 0.055	<0.001*				
	Reference-Restored	51 ± 0.067	<0.001*				
Nov 2017	Control-Reference	2.7 ± 0.45	<0.001*			24 ± 0.46	<0.001*
	Control-Restored	38 ± 0.48	<0.001*			47 ± 0.48	<0.001*
	Reference-Restored	41 ± 0.49	<0.001*			23 ± 0.47	<0.001*
Nov 2018	Control-Reference	1.9 ± 0.15	<0.001*	3.8 ± 0.4	<0.001*		
	Control-Restored	2.6 ± 0.15	<0.001*	5.4 ± 0.44	<0.001*		
	Reference-Restored	0.63 ± 0.11	<0.001*	1.5 ± 0.36	<0.001*		

* Significant at $\alpha = 0.05$.

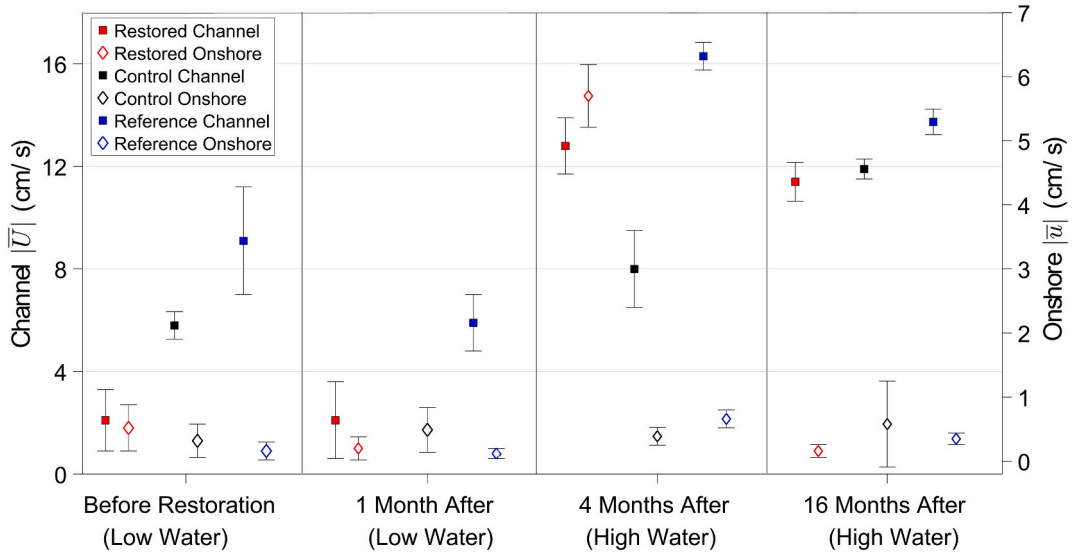

Fig. 3. Mean ± 1 SD observed channel velocities with shoreline velocities on second axis.

cm/s) than the vegetated shorelines for comparable channel velocities (11.9 ± 0.4 cm/s).

3.2. Waves

The ambient wave climate was mild throughout all sampling periods with mean significant wave heights in the channel typically measuring between 0.5 and 3 cm (Table A3). However, four months after restoration, mean significant wave heights observed in the channel of the Restored site were much greater (6.8 ± 0.6 cm). Wind speeds recorded at the Restored site were 8–13 km/h, the highest wind speeds recorded during the study. As waves moved from the channel onto the shore, wave heights generally decreased (Fig. 4a) and wave periods remained static in all sites (Table A3). The lowest wave attenuation rates (11.4 ± 7.1% mean reduction in significant wave height from channel to shore) were observed in the Control site. Waves were more strongly attenuated in the Reference site, with mean attenuation of 35.8 ± 5.7%. Wave attenuation rates in the Reference and Control sites were relatively stable across observation periods and varied only slightly with changes in water level. However, in the Restored site, wave attenuation rate varied substantially with water level (Fig. 4b). When water levels were 5 cm above the wave break structure, attenuation levels (41.8 ± 3.4%) were similar to those observed in the Reference site. As water levels over the structure dropped, attenuation rates increased dramatically to a maximum of 82.6% when the water level was 1 cm below the crest of the wave break structure.

3.3. Boat wakes

Boating traffic was frequent. Wakes propagating toward the shoreline produced shoreline waves that exceeded wind-driven wave heights (Fig. A8a, b) and velocities by well over an order of magnitude. Wakes generated from experimental boat passes exhibited variation in mean wake height within the channel (5.5–12 cm), with larger channel waves corresponding with shallower channel depths. Channel boat wake heights were largest at the Reference site (10.3 ± 1.1 cm), followed by

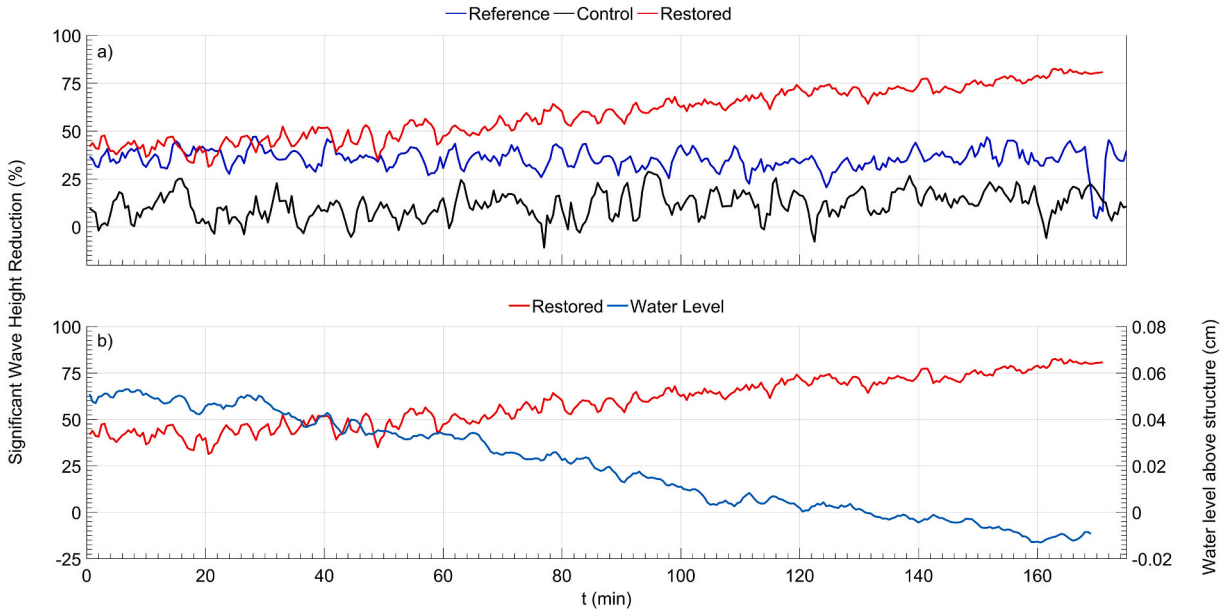

Fig. 4. Wave attenuation: a) across all sites four months after restoration b) in the Restored site with water height relative to breakwaters on second axis.

the Control site (8.8 ± 1.0 cm), and the lowest waves were recorded in the Restored site (7.3 ± 1.1 cm). Despite differences in the channel wake amplitudes, wake amplitudes at the shoreline were similar in magnitude, ranging from 5.56–5.79 cm (Fig. A9), reflecting relative mean attenuation rates of 23% in the Restored shoreline to 46% in the Reference shoreline.

3.4. Turbulence dissipation rates

Four months after restoration, the greatest turbulence dissipation rate for ambient flow conditions was observed in the Restored site ($5.2{\cdot}10^{-5} \pm 5.4{\cdot}10^{-5}$ m^2/s^3). Dissipation was more than an order of magnitude greater than that observed in the Reference ($2.9{\cdot}10^{-6} \pm 2.2{\cdot}10^{-6}$ m^2/s^3) and Control sites ($1.1{\cdot}10^{-6} \pm 1.0{\cdot}10^{-6}$ m^2/s^3) (Table 3). However, as noted above, shoreline velocities and wave heights in the Restored site at this time were over an order of magnitude greater than those observed in the other two sites. With variations of incoming flow conditions, dissipation rates normalized by the prevailing flow condition, in the form of shoreline root-mean-square flow velocities $\left(\varepsilon/\sqrt{u_{rms}^2+v_{rms}^2}\right)$, may offer better comparison across sites. Normalized dissipation rate was greatest in the Reference shoreline (0.20 ± 0.15 m^{-1}) followed by the Restored (0.13 ± 0.13 m^{-1}) and the Control (0.070 ± 0.038 m^{-1}) shorelines (Table 3).

During controlled boat-wake events, 16 months after restoration, turbulence dissipation rates follow closely with onshore-directed velocity and shoreline significant wave heights (Fig. 5). Turbulence dissipation rate responses to changes in the prevailing flow condition are highly non-linear. For example, a threefold increase in significant wave height leads to a two orders of magnitude increase in turbulence dissipation rate (Fig. 5). For wake events, normalized dissipation rates were higher in the Restored (0.037 ± 0.036 m^{-1}) and Reference shorelines (0.050 ± 0.048 m^{-1}) than in the Control shoreline (0.011 ± 0.013 m^{-1}) (Fig. 6, Table 3).

4. Discussion

4.1. Effects of breakwater structure and vegetation on shoreline hydrodynamics

The aim of this study was to detect early hydrodynamic changes following implementation of a living shoreline. The sites were not replicates and were selected to assess impacts of the restoration. Immediately following restoration, shoreline velocities in the Restored site decreased considerably (mean 62% decrease, Fig. A3b). As vegetation densities immediately after restoration were low (three plants per m length of breakwater structure), vegetation was unlikely to have significantly altered flows. Therefore, the immediate hydrodynamic effects more strongly reflect flow interaction with the breakwater structure. At four months post-restoration, mean shoreline velocities in the Restored shoreline increased by over an order of magnitude, far exceeding seasonal changes observed in the other sites (Fig. 3, Fig. A4). While the structure effectively blocked flows during low water levels,

Table 3
Dissipation statistics during ambient conditions (2017) and boat wake passes (2018).

	Site	Normalized Dissipation rate ± SD (m^{-1})	Actual Dissipation rate ± SD (m^2/s^3)
Ambient	Reference	0.20 ± 0.15	$3.4 \cdot 10^{-6} \pm 7.3 \cdot 10^{-6}$
	Control	0.070 ± 0.038	$1.1 \cdot 10^{-6} \pm 1.0 \cdot 10^{-6}$
	Restored	0.13 ± 0.13	$5.2 \cdot 10^{-5} \pm 5.4 \cdot 10^{-5}$
Boat Wakes	Reference	0.050 ± 0.048	$2.2 \cdot 10^{-5} \pm 3.6 \cdot 10^{-5}$
	Control	0.011 ± 0.013	$1.6 \cdot 10^{-6} \pm 1.9 \cdot 10^{-6}$
	Restored	0.037 ± 0.036	$1.1 \cdot 10^{-5} \pm 1.2 \cdot 10^{-5}$

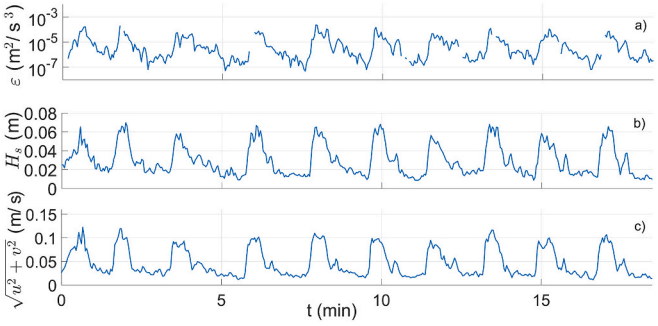

Fig. 5. Boat wake passes at the Reference site with a) dissipation rate (ε, ε obtained from low quality measurements were removed), b) significant wave height (H_s), and c) shoreline mean horizontal velocity. Dissipation rate correlates with wake events and increased energy produced during energetic boat passes.

flow-structure interactions when water levels overtopped the structure and the stronger waves during this sampling period are the likely cause of high velocities recorded in the Restored site. Sixteen months after restoration, flow attenuation in the Restored site was similar to that observed in the Reference shoreline. While immediate hydrodynamic effects in the months following restoration were predominantly related to flow-structure interaction, lower shoreline velocities observed 16 months after restoration may reflect combined effects of both the structure and vegetation. The different outcomes observed over one year's time likely demonstrate the need for living shoreline to attain sufficient densities of vegetation to create desired hydrodynamic conditions.

The opposing hydrodynamic effects observed 4 and 16 months after restoration indicate that the two components of the living shoreline (breakwater structure and vegetation) provided different mechanisms of flow alteration. Following the establishment of shoreline vegetation, incoming flows are altered at the leading edge of the fringe. This alters exerted drag throughout the fringe, imposed by both the vegetation and the shallow bed, and leads to gradual decreases of flow velocity and wave height (e.g., Vasiliki et al., 2011; Paquier et al., 2019). While interaction with the oyster reef structure was dependent on water level, interaction with emergent vegetation provided a more consistent level of flow attenuation. For instance, maximum wind wave attenuation levels (83%) were achieved when water levels were below the structure crest. When water levels were 4–5 cm above the structure crest, wave attenuation rates fell to 43.5 ± 4.7%, which was similar to attenuation rates observed within the mature mangrove vegetation in the Reference shoreline. Chowdhury et al. (2019) observed similar water level dependence on wave attenuation by artificial oyster breakwater reefs in Bangladesh. At water levels below the reef crest, waves were almost completely attenuated, while attenuation at higher water levels depended on the wave height. Small waves were not affected by the artificial oyster reefs when water levels were more than 40 cm above the reef. This is similar to findings of Wiberg et al. (2019), who observe minimal wave attenuation when water levels exceeded 25 cm above the crest of natural intertidal oyster reefs. Analysis by Morris et al. (2021) of wave attenuation by 15 artificial oyster reefs deployed as living shorelines along the Atlantic and Gulf coasts of the U.S. reached similar conclusions, finding that reefs positioned in water depths that maximized oyster recruitment potential did not attenuate waves significantly better than control shorelines. High rates of wave attenuation (mean 68%) were observed only in reefs that were exposed more than 50% of the time.

Living shoreline was less efficient at reducing boat wake energy as compared to mature mangrove. Sixteen months after restoration, the living shoreline reduced boat wake height by a mean 23%, as compared to a mean 46% in mature mangrove forest. This is lower than the mean

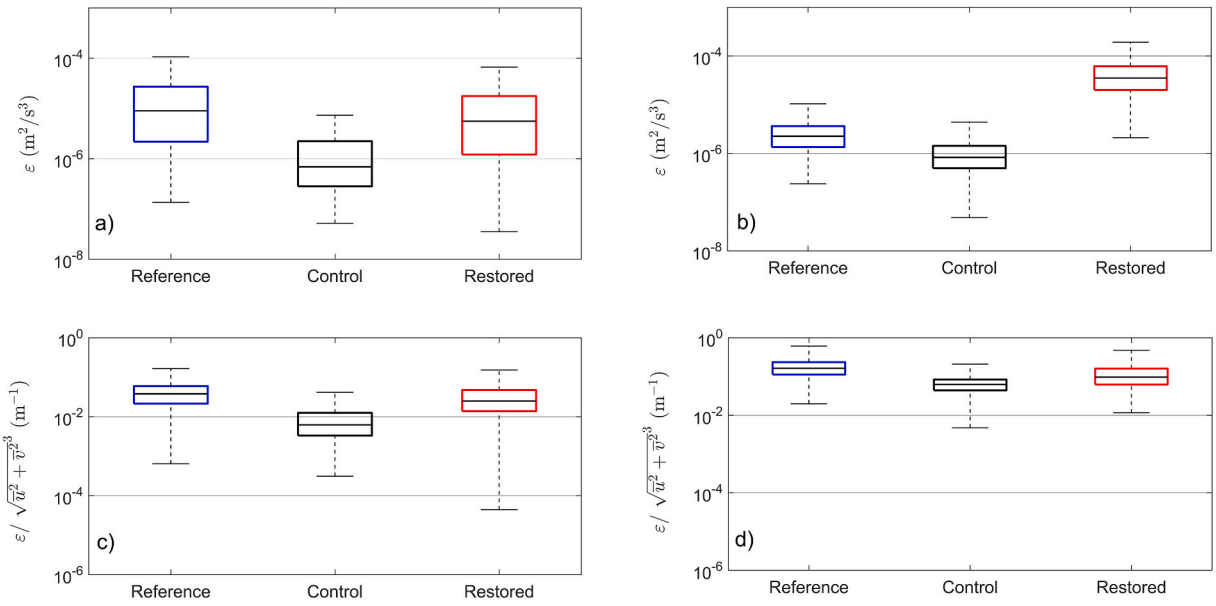

Fig. 6. Observed turbulence dissipation rate (ε) during: a) boat wake passes and b) ambient conditions; normalized turbulence dissipation rate during c) boat wake passes and d) ambient conditions.

ambient wind wave attenuation rate, and also lower than attenuation associated with established emergent vegetation (*Spartina*) and live oysters observed in a flume experiment, wherein 67% of energy from simulated boat wakes was attenuated (Manis et al., 2015). Notably, live oyster recruitment was associated with greater attenuation rates in the flume study. Similarly, Kitsikoudis et al. (2020) observed that canopies of live oyster attenuate flows more efficiently as compared to degraded reef with few live oysters. Live oysters were not observed to have recruited to the oyster shell breakwaters during this study.

4.2. Turbulence dissipation in vegetated shorelines

Turbulence dissipation rate can be considered an indicator of roughness experienced by the flow. High rates of turbulence dissipation suggest that adjacent and upstream obstructions generate turbulence, however prevailing flow conditions are also influential to dissipation rate. During ambient flow conditions four months after restoration, direct comparison of the observed dissipation rates does not provide conclusive indication for which site exhibits greater turbulence dissipation, since there was large flow variability across sites. The ratio of dissipation to the root-mean-square of shoreline velocity (normalized dissipation) was greater at sites with flow obstructions (Reference and Restored sites), which may suggest that turbulent eddies are formed from interaction with either the structure or vegetation, elevating turbulence intensity as compared to the unimpeded flows in the Control site. The experimental boat wake data provided a narrower range of flow conditions, allowing for direct comparisons of turbulence dissipation across sites. Experimental boat passes were completed when wind waves were negligible and at tidal stagnation when current velocities were very low. Hence, the induced turbulence dissipation rates are attributed solely to the boat wakes and correlate well with significant wave heights and orbital velocities (Fig. 5). Normalized and observed dissipation rates during wake events in the Restored and Reference sites surpassed those observed at the unobstructed Control site by an order of magnitude, which is an expected finding. Similarly elevated turbulence dissipation rates were observed during ambient conditions in living shoreline vegetation (6 years after restoration) as compared to a bare shoreline with a seawall (Kibler et al., 2019). However, as in this study, greatest dissipation rates were observed in mature mangrove vegetation.

Given the dependence of turbulence dissipation on the energetics of the prevailing flow, it is expected that dissipation rates should be greater during high-stress events (e.g. boat wake events) as compared to ambient flow conditions. This is indeed observed; however, we also observe that turbulence dissipation rate increases with prevailing flow at a much greater rate in the Reference vegetation (almost fourfold) as compared to the unobstructed Control shoreline (less than 50%) (Table 3). This divergent behavior implies that despite the drop in velocity within mangrove vegetation, suspended sediments entering the fringe of a red mangrove forest may remain in suspension, carried by high turbulence, until both velocity and turbulence are diminished farther landwards. Similarly, Norris et al. (2017) observe that elevated turbulence in the fringe of black mangrove pneumatophores should maintain sediment suspension until deposition occurs within the forest interior. A similar mechanism may account for the high accretion rates observed landward of the breakwater structures in the Restored site.

Rates of dissipation at the three sites ranged from a low of $4.3 \cdot 10^{-8}$ m^2/s^3 at the Control site to maximum of $5.3 \cdot 10^{-4}$ m^2/s^3 at the Restored site. Within the red mangroves of the Reference site, rates ranged from $2.1 \cdot 10^{-7}$ to $2.4 \cdot 10^{-5}$ m^2/s^3 for ambient flow conditions. This is the first comprehensive turbulence dataset obtained from field measurements within red mangroves. Norris et al. (2019) conducted field measurements with similar instrumentation within pneumatophores of black mangroves and reported turbulence dissipation rates up to $6.5 \cdot 10^{-4}$ m^2/s^3 in a much more energetic flow environment. However, it should be noted that the pneumatophores of black mangroves have a different canopy structure than the prop roots of red mangroves, which may account for dissipation differences. Horstman et al. (2018) indicated that idealized uniform mimic vegetation (wooden dowels) used in flume experiments significantly overestimated turbulent stresses when compared to natural pneumatophores, as cross-sectional heterogeneity of the latter distorts shear layer formation at the top of the canopy. This could have significant implications to sediment accretion in that mangrove fringes may actually be more efficient in trapping sediment as compared to models developed in idealized flume studies (Horstman et al., 2018). Flow within idealized surrogates of red mangrove prop roots has been investigated in flume experiments by Shan et al. (2019) and Mazda et al. (1997) who observed maximum TKE at the top of the prop roots due to a shear layer that formed from the rapid increase in flow blockage area from the prop roots stemming from the main trunk. However, prop roots in nature (such as the ones observed herein) may be

fouled by organisms that effect cross-sectional area and processes of flow separation, with influence to eddy shedding. This could result in alteration of turbulence levels in the wake of the prop roots, which will affect sediment suspension and deposition. As a result, more field data are needed to investigate if the presence of biofouling could lead to deviation from predictive formulae related to flow – cylinder interaction.

4.3. Resilience of living shoreline through an extreme event

Conditions observed in the Restored site after Hurricane Irma reinforce conclusions reported by others (Smith et al., 2017, 2018) regarding the potential for nature-based solutions to be resilient to extreme events. Despite the extreme conditions shortly after living shoreline implementation, vegetation mortality and damage to the breakwater structure was not observed. Vegetation coverage at the Restored site increased from before to after Hurricane Irma (Fig. A1). Prior to restoration and the hurricane, sediments of the Restored shoreline were coarse relative to both Reference and Control shorelines (Fig. A5). However, following the hurricane, coarse fractions on the Restored shoreline fell to the lowest levels among all of the sites. This was visually observed as deposition of sand in the lee of the breakwater structure and confirmed by bulk sediment sampling. In addition, following the hurricane, organic content within sediments of the Restored shoreline increased by 360% relative to pre-restoration values. The increase in organic material could derive from either accumulation of particulate organic detritus deposited on the shoreline, or root growth associated with plantings. Given the decrease in organic matter content observed at the Restored site the following year, when vegetation was more prevalent, it is possible that organic debris accumulation behind the breakwater structure was the predominant mechanism for the relatively high carbon content observed after the hurricane.

4.4. Implementation of living shoreline to maximize beneficial hydrodynamic effects

Results of this study detail the transitional stages of hydrodynamic change following living shoreline implementation, which can guide design and implementation of future projects. As this study only documents early stages after implementation based on few observation periods, conclusions about the long-term stability of the site cannot be reached. However, study results may be helpful to set realistic early-stage expectations for living shoreline hydrodynamic impacts. Hydrodynamic effects related to strong flow-vegetation interaction were not observed until more than a year after living shoreline implementation. The hydrodynamic environment observed at early stages after implementation was related to flow interaction with the oyster reef structure. Similar transient conditions may occur in other new projects that combine vegetation and breakwater structures. Given the dependence of shoreline hydrodynamics on water level relative to the structure crest, oyster reef structure design and deployment location should be assessed in conjunction with tidal and seasonal water level variation, as well as balance between shoreline engineering objectives (wave attenuation) and ecological objectives (oyster recruitment) (Morris et al., 2019). Gaps in breakwater structures for wildlife passage are often required by permits but have been noted as locations of local scour in living shoreline projects (Polk and Eulie, 2018). Local scour within and in the lee of gaps was observed, demonstrating the potential for edge effects and spatial heterogeneity in sediment deposition. However, net sediment deposition landward of the breakwater structure was extensive enough to preclude sampling at low water levels one year after implementation, suggesting that early hydrodynamic conditions were suitable to promote deposition until vegetation had grown sufficiently to alter flows.

5. Conclusion

This is the first before-after controlled study of early hydrodynamic impacts attributed to living shoreline stabilization. Changes to shoreline vegetation, hydrodynamic environment, and benthic sediments were observed over a 16-month period that included implementation of a living shoreline (comprised of an oyster shell breakwater structure and planted marsh grasses and mangroves) and its performance in the wake of an extreme event weeks after implementation. Immediately after stabilization, when planted vegetation was sparse, the interaction of flows with the oyster shell breakwater structure dominated shoreline hydrodynamics. When water levels were below the breakwater crest elevation, shoreline velocities at the Restored site decreased by 62% relative to pre-restoration levels. However, sampling at higher water levels revealed a considerable increase in shoreline velocities, a phenomenon that was not observed in control sites and is attributed to wave transmission over the breakwater structure. Similarly, wave attenuation was greatest at the Restored site when water levels were below breakwater crest height. Sixteen months after restoration, dense growth of *S. alterniflora* in the Restored shoreline reduced shoreline velocities. Turbulence dissipation rates observed in the vegetated Reference and Restored sites were an order of magnitude greater than in the unvegetated Control site during high-stress boat wake events. This study suggests that living shorelines can be resilient to extreme events, even shortly after their deployment. Following Hurricane Irma, organic matter content in shoreline sediments increased threefold at the Restored site and shoreline sediments became finer. Given the strong role of flow-structure interaction in shaping the shoreline hydrodynamic environment immediately after living shoreline stabilization, it is recommended that living shoreline design should carefully consider local hydrodynamic forcings and inundation depths given local tidal and seasonal water level ranges, particularly when placing breakwater structures. Future research regarding breakwater structure optimal characteristics, structural designs, and placement appropriate for different tidal regimes may assist managers with optimal protection of planted vegetation and seaward growth of degrading shoreline.

Declaration of Competing Interest

The authors declare that they have no known competing financial interests or personal relationships that could have appeared to influence the work reported in this paper.

Acknowledgments

We would like to acknowledge Iris Peterson and Samantha Maldonado for sediment data analysis, Spencer Shannon for his review, and Barbara Nogueira Tirado, Arash Aliabadi Farahani, and Samantha Maldonado for field assistance. Funding for this research was provided by the US National Science Foundation, grant number 1617374.

Appendix A. Supplementary data

Supplementary data to this article can be found online at https://doi.org/10.1016/j.ecoleng.2021.106306.

References

Arkema, Katie K., Verutes, Gregory M., Wood, Spencer A., Clarke-Samuels, Chantalle, Rosado, Samir, Canto, Maritza, Rosenthal, Amy, et al., 2015. Embedding ecosystem services in coastal planning leads to better outcomes for people and nature. Proc. Natl. Acad. Sci. 112 (24), 7390–7395.

Barbier, Edward B., Hacker, Sally D., Kennedy, Chris, Koch, Evamaria W., Stier, Adrian C., Silliman, Brian R., 2011. The value of estuarine and coastal ecosystem services. Ecol. Monogr. 81 (2), 169–193.

Bilkovic, D.M., Mitchell, M.M., Toft, J.D., La Peyre, M.K. (Eds.), 2017. Living Shorelines: The Science and Management of Nature-Based Coastal Protection. CRC Press, Taylor and Francis Group, Boca Raton, FL.

Bouma, T.J., De Vries, M.B., Low, E., Kusters, L., Herman, P.M.J., Tanczos, I.C., Temmerman, S., Hesselink, A., Meire, P., Van Regenmortel, S., 2005. Flow hydrodynamics on a mudflat and in salt marsh vegetation: identifying general relationships for habitat characterisations. Hydrobiologia 540 (1–3), 259–274.

Bozek, Catherine M., Burdick, David M., 2005. Impacts of seawalls on saltmarsh plant communities in the Great Bay Estuary, New Hampshire USA. Wetl. Ecol. Manag. 13 (5), 553–568.
Brockmeyer, R.E., Rey, J.R., Virnstein, R.W., Gilmore, R.G., Earnest, L., 1996. Rehabilitation of impounded estuarine wetlands by hydrologic reconnection to the Indian River Lagoon, Florida (USA). Wetl. Ecol. Manag. 4 (2), 93–109.
Campbell, Donna, 2015. Quantifying the effects of boat wakes on intertidal oyster reefs in a shallow estuary. In: Electronic Theses and Dissertations, 2004-2019, 58.
Cangialosi, John P., Latto, Andrew S., Berg, Robbie, 2018. National Hurricane Center Tropical Cyclone Report: Hurricane Irma. National Oceanic and Atmospheric Administration (May, 30).
Chmura, Gail L., 2009. Tidal salt marshes. In: The Management of Natural Coastal Carbon Sinks. IUCN Gland, Switzerland.
Chmura, Gail L., Anisfeld, Shimon C., Cahoon, Donald R., Lynch, James C., 2003. Global carbon sequestration in tidal, saline wetland soils. Glob. Biogeochem. Cycles 17 (4).
Chowdhury, Mohammed Shah Nawaz, Walles, Brenda, Sharifuzzaman, S.M., Hossain, M. Shahadat, Ysebaert, Tom, Smaal, Aad C., 2019. Oyster breakwater reefs promote adjacent mudflat stability and salt marsh growth in a monsoon dominated subtropical coast. Sci. Rep. 9, 8549.
Coen, Loren D., Luckenbach, Mark W., Breitburg, Denise L., 1999. The role of oyster reefs as essential fish habitat: a review of current knowledge and some new perspectives. In: American Fisheries Society Symposium, 22, pp. 438–454.
Davis, Jana L.D., Takacs, Richard L., Schnabel, Robert, 2006. Evaluating ecological impacts of living shorelines and shoreline habitat elements: an example from the upper western Chesapeake Bay. In: Management, Policy, Science, and Engineering of Nonstructural Erosion Control in the Chesapeake Bay, 55.
Dosskey, M.G., Vidon, P., Gurwick, N.P., Allan, C.J., Duval, T.P., Lowrance, R., 2010. The role of riparian vegetation in protecting and improving chemical water quality in streams. J. Am. Water Resour. Assoc. 46 (2), 261–277.
Down, Cherie, Withrow, R., 1978. Vegetation and Other Parameters in the Brevard County Bar-Built Estuaries.
Garvis, Stephanie K., Sacks, Paul E., Walters, Linda J., 2015. Formation, movement, and restoration of dead intertidal oyster reefs in Canaveral National Seashore and Mosquito Lagoon, Florida. J. Shellfish Res. 34 (2), 251–259.
Gedan, K.B., Kirwan, M.L., Wolanski, E., Barbier, E.B., Silliman, B.R., 2011. The present and future role of coastal wetland vegetation in protecting shorelines: answering recent challenges to the paradigm. Clim. Change 106 (1), 7–29.
Gittman, Rachel K., Peterson, Charles H., Currin, Carolyn A., Fodrie, F. Joel, Piehler, Michael F., Bruno, John F., 2016a. Living shorelines can enhance the nursery role of threatened estuarine habitats. Ecol. Appl. 26 (1), 249–263.
Gittman, Rachel K., Scyphers, Steven B., Smith, Carter S., Neylan, Isabelle P., Grabowski, Jonathan H., 2016b. Ecological consequences of shoreline hardening: a meta-analysis. BioScience 66 (9), 763–773.
Goring, Derek G., Nikora, Vladimir I., 2002. Despiking acoustic Doppler velocimeter data. J. Hydraul. Eng. 128 (1), 117–126.
Grabowski, Jonathan H., Brumbaugh, Robert D., Conrad, Robert F., Keeler, Andrew G., Opaluch, James J., Peterson, Charles H., Piehler, Michael F., Powers, Sean P., Smyth, Ashley R., 2012. Economic valuation of ecosystem services provided by oyster reefs. BioScience 62 (10), 900–909.
Griggs, Gary B., 2005. The impacts of coastal armoring. Shore Beach 73 (1), 13–22.
Herbert, Deidre, Astrom, Emily, Bersoza, Ada, Batzer, Audrey, McGovern, Patrick, Angelini, Christine, Wasman, Scott, Dix, Nicole, Sheremet, Alex, 2018. Mitigating erosional effects induced by boat wakes with living shorelines. Sustainability 10 (2), 436.
Horstman, Erik, Dohmen-Janssen, Marjolein, Narra, Pedro, van den Berg, Niels-Jasper, Siemerink, Martijn, Balke, Thorsten, Bouma, Tjeerd, Hulscher, Suzanne, 2012. Wave attenuation in mangrove forests; field data obtained in Trang, Thailand. In: McKee-Smith, J., Lynett, P. (Eds.), Proceedings of 33rd International Conference on Coastal Engineering Proceedings, 1. Santander, p. 40 (33).
Horstman, Erik M., Marjolein Dohmen-Janssen, C., Hulscher, Suzanne J.M.H., 2013. Flow routing in mangrove forests: a field study in Trang province, Thailand. Cont. Shelf Res. 71, 52–67.
Horstman, E.M., Dohmen-Janssen, Catarine M., Narra, P.M.F., Van den Berg, N.J.F., Siemerink, M., Hulscher, Suzanne J.M.H., 2014. Wave attenuation in mangroves: a quantitative approach to field observations. Coast. Eng. 94, 47–62.
Horstman, E.M., Bryan, K.R., Mullarney, J.C., Pilditch, C.A., Eager, C.A., 2018. Are flow-vegetation interactions well represented by mimics? A case study of mangrove pneumatophores. Adv. Water Resour. 111, 360–371.
Kibler, Kelly M., Kitsikoudis, Vasileios, Donnelly, Melinda, Spiering, David W., Walters, Linda, 2019. Flow–vegetation interaction in a living shoreline restoration and potential effect to Mangrove recruitment. Sustainability 11 (11), 3215.
Kitsikoudis, Vasileios, Kibler, Kelly M., Walters, Linda J., 2020. In-situ measurements of turbulent flow over intertidal natural and degraded oyster reefs in an estuarine lagoon. Ecol. Eng. 143, 105688.
Lanckriet, Thijs, Puleo, Jack A., 2013. Near-bed turbulence dissipation measurements in the inner surf and swash zone. J. Geophys. Res. Oceans 118 (12), 6634–6647.
Larsen, Laurel G., Harvey, Judson W., 2010. How vegetation and sediment transport feedbacks drive landscape change in the Everglades and wetlands worldwide. Am. Nat. 176 (3), E66–E79.
Manis, Jennifer E., Garvis, Stephanie K., Jachec, Steven M., Walters, Linda J., 2015. Wave attenuation experiments over living shorelines over time: a wave tank study to assess recreational boating pressures. J. Coast. Conserv. 19 (1), 1–11.
Maul, George A., 2015. Florida's rising seas: A report in feet per century for coastal interests. Florida Sci. 78 (2), 64–76.
Mazda, Yoshihiro, Wolanski, Eric, King, Brian, Sase, Akira, Ohtsuka, Daisuke, Magi, Michimasa, 1997. Drag force due to vegetation in mangrove swamps. Mangrove Salt Marshes 1 (3), 193–199.
McConchie, J.A., Toleman, I.E.J., 2003. Boat wakes as a cause of riverbank erosion: a case study from the Waikato River, New Zealand. J. Hydrol. N. Z. 163–179.
McGranahan, Gordon, Balk, Deborah, Anderson, Bridget, 2007. The rising tide: assessing the risks of climate change and human settlements in low elevation coastal zones. Environ. Urban. 19 (1), 17–37.
Mcleod, Elizabeth, Chmura, Gail L., Bouillon, Steven, Salm, Rodney, Björk, Mats, Duarte, Carlos M., Lovelock, Catherine E., Schlesinger, William H., Silliman, Brian R., 2011. A blueprint for blue carbon: toward an improved understanding of the role of vegetated coastal habitats in sequestering CO2. Front. Ecol. Environ. 9 (10), 552–560.
Miles, Jonathon R., Russell, Paul E., Huntley, David A., 2001. Field measurements of sediment dynamics in front of a seawall. J. Coast. Res. 17 (1), 195–206.
Mitra, Abhijit, Zaman, Sufia, 2015. Blue carbon in faunal community. In: Blue Carbon Reservoir of the Blue Planet. Springer, pp. 203–226.
Morris, Rebecca L., Bilkovic, Donna M., Boswell, Maura K., Bushek, David, Cebrian, Just, Goff, Joshua, Kibler, Kelly M., La Peyre, M.K., McClenachan, G., Moody, J., Sacks, P., 2019. The application of oyster reefs in shoreline protection: are we over-engineering for an ecosystem engineer? J. Appl. Ecol. 56 (7), 1703–1711.
Morris, R.L., La Peyre, M.K., Webb, B.M., Marshall, D.A., Bilkovic, D.M., Cebrian, J., Swearer, S.E., 2021. Large-scale variation in wave attenuation of oyster reef living shorelines and the influence of inundation duration. Ecol. Appl. e2382.
Nepf, H.M., 1999. Drag, turbulence, and diffusion in flow through emergent vegetation. Water Resour. Res. 35 (2), 479–489.
Nepf, H.M., 2012. Flow and transport in regions with aquatic vegetation. Annu. Rev. Fluid Mech. 44, 123–142.
Neumeier, U.R.S., Amos, Carl L., 2006. The influence of vegetation on turbulence and flow velocities in European salt-marshes. Sedimentology 53 (2), 259–277.
Nicholls, Robert J., Cazenave, Anny, 2010. Sea-level rise and its impact on coastal zones. Science 328 (5985), 1517–1520.
Nicholls, Robert J., Hoozemans, Frank M.J., Marchand, Marcel, 1999. Increasing flood risk and wetland losses due to global sea-level rise: regional and global analyses. Glob. Environ. Chang. 9, S69–S87.
Norris, Benjamin K., Mullarney, Julia C., Bryan, Karin R., Henderson, Stephen M., 2017. The effect of pneumatophore density on turbulence: a field study in a Sonneratia-dominated mangrove forest, Vietnam. Cont. Shelf Res. 147, 114–127.
Norris, B.K., Mullarney, J.C., Bryan, K.R., Henderson, S.M., 2019. Turbulence within natural mangrove pneumatophore canopies. J. Geophys. Res. Oceans 124 (4), 2263–2288.
Paquier, A.E., Meulé, S., Anthony, E.J., Larroudé, P., Bernard, G., 2019. Wind-induced hydrodynamic interactions with aquatic vegetation in a fetch-limited setting: Implications for coastal sedimentation and protection. Estuar. Coasts 42 (3), 688–707.
Peyre, La, Megan, K., Humphries, Austin T., Casas, Sandra M., La Peyre, Jerome F., 2014. Temporal variation in development of ecosystem services from oyster reef restoration. Ecol. Eng. 63, 34–44.
Piazza, Bryan P., Bank, Patrick D., La Peyre, Megan K., 2005. The potential for created oyster shell reefs as a sustainable shoreline protection strategy in Louisiana. Restor. Ecol. 13 (3), 499–506.
Plant, Nathaniel G., Griggs, Gary B., 1992. Interactions between nearshore processes and beach morphology near a seawall. J. Coast. Res. 183–200.
Polk, Mariko A., Eulie, Devon O., 2018. Effectiveness of living shorelines as an erosion control method in North Carolina. Estuar. Coasts 41 (8), 2212–2222.
Ridge, Justin T., Rodriguez, Antonio B., Fodrie, F. Joel, 2017. Salt marsh and fringing oyster reef transgression in a shallow temperate estuary: Implications for restoration, conservation and blue carbon. Estuar. Coasts 40 (4), 1013–1027.
Scyphers, Steven B., Powers, Sean P., Heck Jr., Kenneth L., Byron, Dorothy, 2011. Oyster reefs as natural breakwaters mitigate shoreline loss and facilitate fisheries. PLoS One 6 (8), e22396.
Shan, Y., Liu, C., Nepf, H., 2019. Comparison of drag and velocity in model mangrove forests with random and in-line tree distributions. J. Hydrol. 568, 735–746.
Smith, Carter S., Gittman, Rachel K., Neylan, Isabelle P., Scyphers, Steven B., Morton, Joseph P., Fodrie, F. Joel, Grabowski, Jonathan H., Peterson, Charles H., 2017. Hurricane damage along natural and hardened estuarine shorelines: using homeowner experiences to promote nature-based coastal protection. Mar. Policy 81, 350–358.
Smith, Carter S., Puckett, Brandon, Gittman, Rachel K., Peterson, Charles H., 2018. Living shorelines enhanced the resilience of saltmarshes to Hurricane Matthew (2016). Ecol. Appl. 28 (4), 871–877.
Stocker, Thomas F., Qin, Dahe, Plattner, Gian-Kasper, Tignor, Melinda, Allen, Simon K., Boschung, Judith, Nauels, Alexander, Yu, Xia, Bex, Vincent, Midgley, Pauline M., 2013. Climate Change 2013: The Physical Science Basis, Contribution of Working Intergovernmental Panel of Climate Change.
Stocking, Jonathan B., Rippe, John P., Reidenbach, Matthew A., 2016. Structure and dynamics of turbulent boundary layer flow over healthy and algae-covered corals. Coral Reefs 35 (3), 1047–1059.
Tebaldi, Claudia, Strauss, Benjamin H., Zervas, Chris E., 2012. Modelling Sea level rise impacts on storm surges along US coasts. Environ. Res. Lett. 7 (1), 014032.
Temmerman, S., Bouma, T.J., Govers, G., Zheng, B.W., De Vries, M.B., Herman, P.M.J., 2005. Impact of vegetation on flow routing and sedimentation patterns: Three-dimensional modeling for a tidal marsh. J. Geophys. Res. Earth Surf. 110 (F4).
Thomas, R.E., Schindfessel, L., McLelland, S.J., Creëlle, S., De Mulder, T., 2017. Bias in mean velocities and noise in variances and covariances measured using a multistatic acoustic profiler: the Nortek Vectrino Profiler. Meas. Sci. Technol. 28 (7), 075302.

Tinoco, R.O., Coco, G., 2018. Turbulence as the main driver of resuspension in oscillatory flow through vegetation. J. Geophys. Res. Earth Surf. 123 (5), 891–904.
Vasiliki, Stratigaki, Manca, Eleonora, Prinos, Panayotis, Losada, Inigo J., Lara, Javier L., Sclavo, Mauro, Amos, Carl L., Cáceres, Iván, Sánchez-Arcilla, Agustín, 2011. Large-scale experiments on wave propagation over Posidonia oceanica. J. Hydraul. Res. 49 (sup1), 31–43.
Vidon, P.G., Hill, A.R., 2004. Landscape controls on nitrate removal in stream riparian zones. Water Resour. Res. 40 (3).
Wahl, T.L., 2003. Discussion of "Despiking acoustic doppler velocimeter data" by Derek G. Goring and Vladimir I. Nikora. J. Hydraul. Eng. 129 (6), 484–487.
Wall, Lisa M., Walters, Linda J., Grizzle, Raymond E., Sacks, Paul E., 2005. Recreational boating activity and its impact on the recruitment and survival of the oyster Crassostrea virginica on intertidal reefs in Mosquito Lagoon, Florida. J. Shellfish Res. 24 (4), 965–974.
Walters, Linda J., Roman, A., Stiner, J., Weeks, D., 2001. Water Resource Management Plan, Canaveral National Seashore, 224. National Park Service, Canaveral National Seashore, Titusville, FL.
Wiberg, Patricia L., Taube, Sara R., Ferguson, Amy E., Kremer, Marnie R., Reidenbach, Matthew A., 2019. Wave attenuation by oyster reefs in Shallow Coastal Bays. Estuar. Coasts 42 (2), 331–347.
Wiles, Philip J., Rippeth, Tom P., Simpson, John H., Hendricks, Peter J., 2006. A novel technique for measuring the rate of turbulent dissipation in the marine environment. Geophys. Res. Lett. 33 (21).
Yagci, Oral, Yildirim, Isilsu, Celik, Mehmet Furkan, Kitsikoudis, Vasileios, Duran, Zaide, Ozgur Kirca, V.S., 2017. Clear water scour around a finite array of cylinders. Appl. Ocean Res. 68, 114–129.
Yager, E.M., Schmeeckle, M.W., 2013. The influence of vegetation on turbulence and bed load transport. J. Geophys. Res.: Earth Surf. 118 (3), 1585–1601.
Yang, Judy Q., Nepf, Heidi M., 2018. A turbulence-based bed-load transport model for bare and vegetated channels. Geophys. Res. Lett. 45 (19), 10–428.